

RESEARCH PAPER

NUMERICAL SIMULATION OF BENDING PROCESS FOR STEEL SHEETS USED IN AUTOMOTIVE INDUSTRY WITH EMPHASIS ON SPRINGBACK

Peter Mulidrán^{1)*}, Emil Spišák¹⁾, Miroslav Tomáš¹⁾, Janka Majerníková¹⁾, Vladimír Rohal¹⁾

¹⁾ Institute of Technology and Material Engineering, Faculty of Mechanical Engineering, Technical University of Košice, Mäsiarska 74, 040 01, Košice, Slovakia

* Corresponding author: peter.mulidran@tuke.sk, tel.: +421556023516, Faculty of Mechanical Engineering / Technical University of Košice, 04001, Košice, Slovakia

Received: 29.02.2024

Accepted: 22.03.2024

ABSTRACT

This study examines the influence of material models employed in FE simulations on springback prediction for various steels. The goal is to contribute to the understanding of springback prediction for steels commonly used in automotive manufacturing. In this paper, the springback behavior of TRIP, HSLA, and EDDQ steels following a V-bending operation with a 90° bend angle was analyzed. Numerical simulations utilize both the Hill48 and Barlat89 yield criteria, combined with the Ludwik and Swift hardening models. The simulation data against results obtained from physical experiments were compared and evaluated. The obtained experimental findings demonstrate a correlation between springback and mechanical properties, with yield strength playing a significant role. Higher values of yield strength harm the final angle of the bent part, thus increasing the springback of the part. The numerical results of the springback were not identical to the experimentally achieved springback values in most cases. Particularly, when Swift hardening model was used in the simulation.

Keywords: springback, automotive steel, numerical simulation, bending, yield criterion

INTRODUCTION

Steel is still an essential material to produce vehicles. It is mainly used for the body structure of vehicles, also drive-train parts and suspension parts can be made of steel. The average passenger vehicle contains around 900 kg of steel. Today, up to 60% of the steel used in passenger cars is high-strength steel. High-strength steel has been used by automobile manufacturers for almost thirty years now. The main reason for using these types of steels is to increase the passive safety of the vehicles and to reduce the weight of these vehicles. The reduction of weight mainly contributes to higher fuel efficiency. However, high-strength steels have lower formability and greater springback in comparison with conventional steels used for drawing, the main reason for that is the higher value of the yield strength and lower ductility of these steels. Furthermore, the development of new and even stronger high-strength steels is ongoing, to achieve even lighter and safer vehicles. Despite the challenges associated with formability and springback, high-strength steel remains a crucial material for the future of car manufacturing [1, 2].

The TRIP steels, or Transformation Induced Plasticity steels, have higher mechanical properties (yield strength and tensile strength) if compared with conventional steels [3]. Strain hardening is also greater; therefore, it offers a superior combination of strength and formability properties which can be attributed to the multiphase structure of these steels. The main characteristic of TRIP steels is that they modify the microstructure during the plastic deformation process as part of the austenite transformation to martensite, with the following change in the material properties. One of the main issues of TRIP steels is strong elastic

recovery, also known as springback, which occurs after forming [4, 5].

The HSLA (high strength low alloy) steels are characterised by low carbon content, typically between 0.02 and 0.04 % and rather low amounts of alloying elements, up to 1,5 %. Therefore, these steels have excellent formability and weldability; both properties are important for the production and joining of car body stampings. Typical alloying elements include Mn, Si, Cr, Ni and Mo. The yield strength of HSLA steels ranges from 250 to 600 MPa and they are used in vehicle production and bridges amongst other applications [6, 7, 8].

The EDDQ steel is a low carbon steel, extra deep drawing quality type, with low strength, a high total elongation of about 50% and a high *r*-value. This steel typically contains less than 0.005 percent carbon and uses a low level of titanium and/or columbium to create an interstitial-free chemistry that produces an extremely refined grain pattern. It is used for the production of car body outer parts, with this type of steel strict surface quality can be maintained [8].

Bending, a widely used manufacturing process involves plastic deformation of the material under the application of a bending moment. Accurate bending of sheet steel requires careful consideration of the material's mechanical properties at the design stage, including elasticity modulus, yield stress, the ratio of yield stress to ultimate tensile stress, and microstructure [9]. The non-uniform strain distribution within the bent section generates residual stress after the external load is removed. This residual stress manifests as springback, an involuntary change in the shape of the formed part.

Springback is quantified by the springback coefficient or angle [10]. A common countermeasure involves designing and

forming tools that account for springback compensation, but determining the exact amount can be challenging even for experienced tool designers, often relying on trial and error. Additionally, using the same tool for different materials is problematic due to their varying mechanical and plastic properties. To achieve the desired dimensional accuracy and assembly ease, specific adjustments need to be made in die design. Other countermeasures against springback include stiffening techniques (embossing or beads), crash forming with a pressure pad, or employing variable blank holder force [7, 8].

Lawanwong et al. [11] introduced a novel technique called "double-action bending" to eliminate springback in stamped parts made of advanced high-strength steel (HSS). They utilized finite element (FE) analysis to optimize process and tool parameters before physical experimentation.

Similarly, industries like automotive manufacturing rely heavily on accurate predictions of the forming process, including stress-strain distribution, springback, and thickness [12]. Today, FE analysis offers a reliable tool for more accurate springback prediction [13, 14]. FE analysis (FEA) is a cutting-edge tool that empowers engineers to achieve precise springback predictions [15, 16].

Numerous researchers have employed experiments and simulations to investigate springback. For instance, Mulidran et al. [17] conducted numerical simulations to predict springback in aluminum alloy A-pillars, utilizing various combinations of yield criteria and hardening laws. The work of Neto et al. [18] focused on wrinkling and springback prediction, particularly the influence of applied boundary conditions in simulations. They also compared the wrinkling tendency between mild steel DC06 and dual-phase steel DP600. Slota et al. [19] investigated the impact of various technological parameters (blank holding force, friction) on springback in U-bending with stretching through numerical simulations using the Hill48 yield criterion and the Hollomon hardening curve. Seo et al. [20] evaluated the effects of different constitutive equations on springback prediction accuracy, utilizing two yield functions (Hill48 and Yld2000) in combination with the Yoshida-Uemori hardening model within FE simulations for U-bend and drawn T-shaped parts made of TRIP steel. Baara et al. [21] developed a new constitutive hardening material model for more accurate springback predictions, aiming to extend the Chord model to replicate the strain recovery point with non-zero residual stress. Cui et al. [22] proposed a novel stamping method termed electromagnetic-assisted stamping (EMAS) to control springback using a magnetic force. Their results demonstrated that increasing discharge voltage reduced the bent angle after springback. Mulidran et al. [23] conducted bending experiments and simulations of deep-drawing quality steel to examine the accuracy of springback prediction. They investigated the impact of material orientation, bending tool geometry, and applied force on the springback of DC06 steel. Their results reveal that blanks cut perpendicular to the rolling direction exhibit less springback compared to those cut parallel, when employing a specific bend radius. Additionally, the experimental and numerical results suggest a potential correlation between increased force and reduced springback.

This study uniquely investigates the impact of material models on springback prediction for V-shaped parts made of TRIP steel used in car body production. Additionally, it evaluates the influence of material models on springback prediction under various process conditions, aiming to broaden the existing knowledge base. The research compares springback prediction results for V-shaped parts made of three different types of steels (EDDQ, HSLA, and TRIP) commonly used in car body production with experimental test results. The springback prediction is conducted using FEA within the Autoform forming simulation software. To perform a comprehensive numerical analysis for different steel sheets, the study employs two types of yield surface

models (Hill48 and Barlat89) in combination with two hardening models (Swift and Ludwik) for springback.

MATERIAL AND METHODS

Experimental procedure

The experimental testing was conducted in the Laboratory of Testing Mechanical Properties, which is part of the Institute of Technology and Material Engineering. Three different types of steel were used in the experiment. The material properties of DC06 steel are presented in **Table 1**. Micro alloyed steel H220 properties are shown in **Table 2**. Properties of steel RAK 40/70 are presented in **Table 3**. Testing of material properties was done according to the standards STN EN ISO 6892-1:2019 Metallic materials - Tensile testing - Part 1: Method of test at room temperature, STN EN ISO 10113: 2020 Metallic materials - Sheet and strip - Determination of plastic strain ratio, and STN EN ISO 10275: 2020 Metallic materials - Sheet and strip - Determination of tensile strain hardening exponent. These tests were performed on the material test machine TIRAtest 2300. This test machine is equipped with a tensometer, longitudinal extensometer, and also with a sensor that is used for measuring the width of the tensile test specimen during testing. Tensile test specimens were prepared according to STN EN ISO 6892-1:2019 standard.

The bending experiments were conducted on hydraulic press ZD-40. This device also consists of a tensometer which was used to measure applied force. The Control unit of ZD-40 collected force data, which were then transferred to PC and later processed in Excel. **Fig. 1** shows a bending tool scheme with dimensions for the experimental testing.

The bending angle, the angle of working surfaces of a bending tool was 90 degrees. The punch with a bending radius $R = 3\text{ mm}$ was used in testing. The blank used for bending had a rectangular shape with dimensions of 90 mm x 40 mm. These specimens were cut 0° rolling direction. The thickness of the DC06, H220 and TRIP blanks were 0.70, 0.75 and 0.85 mm respectively. Blanks were prepared using hydraulic shears LVD CS6/31. The calibration force was approximately two times the applied bending force. For each variable, five specimens were used in the testing.

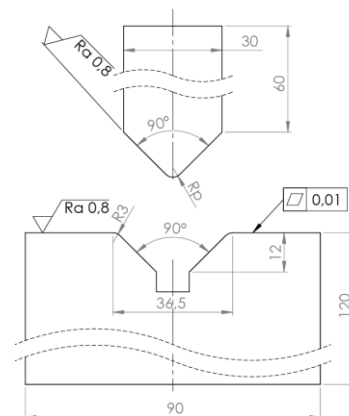


Fig. 1 Bending tool scheme with dimensions

The springback measurement consisted of measuring the arm opening angle β [°] as shown in **Fig. 2**. The stamping image after bending was imported into AutoCAD and the angle between arms was measured.

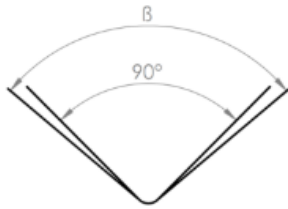


Fig. 2 Measurement of arm opening angle β

Simulation procedure

The numerical simulations of bending TRIP steel sheets were conducted in CAE forming software Autoform R3 which uses a special implicit method and adaptive mesh algorithms. Tool geometry is an important factor in sheet metal forming. Thus it is also important to correctly model forming tools which are then used in CAE software. The imported CAD model of the

experimental tool, which was used in numerical simulation, is pictured in Fig. 3.

The Geometry, dimensions of the CAD model of the tool were the same as in the experimental bending tool. After importing the CAD model into the CAE environment, the tool surfaces needed for simulation were meshed with triangular shell elements. The tools were modeled as rigid bodies. The accuracy of the numerical simulation was set to fine. With this setting, the program automatically generates mesh parameters for blank. Blank also consisted of triangular elements.

The Initial element size of the shell element was set to 3 mm with a maximal refinement level of 2. Radius penetration was set to 0.16; several integration points were set by software to 11. The maximum time step was set to 0.5 s and the coefficient of friction value was set to 0.27. This value was selected because of the higher friction which occurs between zinc-plated steel and tool steel (with no lubrication) compared to friction pair steel-steel [24, 25].

Table 1 Mechanical properties of DC06 steel

Direction [°]	Yield strength σ_y [MPa]	Tensile strength σ_u [MPa]	Young's modulus E [GPa]	Uniform elongation A_{80} [%]	Strain hardening exponent n [-]	Coefficient of normal anisotropy r [-]	Poisson's ratio V [-]
0	145	292	210	50.8	0.258	1.888	0.3
45	151	298	210	47.9	0.255	1.464	0.3
90	149	290	210	48.0	0.259	2.193	0.3

Table 2 Mechanical properties of H220 steel

Direction [°]	Yield strength σ_y [MPa]	Tensile strength σ_u [MPa]	Young's modulus E [GPa]	Uniform elongation A_{80} [%]	Strain hardening exponent n [-]	Coefficient of normal anisotropy r [-]	Poisson's ratio V [-]
0	220	381	210	34.5	0.231	1.170	0.3
45	225	368	210	37.4	0.237	1.780	0.3
90	238	383	210	35.8	0.232	1.820	0.3

Table 3 Mechanical properties of RAK 40/70 steel

Direction [°]	Yield strength σ_y [MPa]	Tensile strength σ_u [MPa]	Young's modulus E [GPa]	Uniform elongation A_{80} [%]	Strain hardening exponent n [-]	Coefficient of normal anisotropy r [-]	Poisson's ratio V [-]
0	441	766	210	27.9	0.293	0.680	0.3
45	442	762	210	25.4	0.294	0.805	0.3
90	445	766	210	25.9	0.278	0.926	0.3

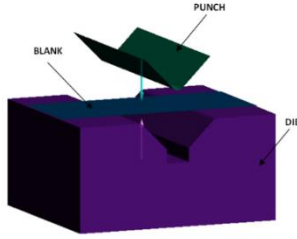


Fig. 3 CAD model of the bending tool used in the simulation

To study the effect of various configurations of constitutive models on the springback results in the FEM simulation Hill48 and Barlat89 yield criteria were used in combination with Ludwik and Swift hardening models in the numerical simulations. In this work, two isotropic hardening rules and two combined hardening rules were tested in numerical simulations. Isotropic hardening rules are defined as:

- Ludwik $\sigma = K \cdot \varphi^n$ (1)
- Swift $\sigma = K \cdot (\varphi_0 + \varphi_{pl})^n$ (2)

where σ is the true stress, K is the strength coefficient, n is the strain hardening exponent, φ_0 is the pre-strain and φ_{pl} is the plastic strain. Material model constants used in both hardening rules are shown in Table 4, 5 and 6.

Table 4 Material constants used for definition of hardening rules of DC06 steel

Model	K [MPa]	φ_0 [-]	n [-]
Ludwik	541	-	0.258
Swift	530	0.00617	0.252

Table 5 Material constants used for definition of hardening rules of H220 steel

Model	K [MPa]	φ_0 [-]	n [-]
Ludwik	673	-	0.231
Swift	634	0.00363	0.225

Table 6 Material constants used for definition of hardening rules of RAK 40/70 steel

Model	K [MPa]	φ_0 [-]	n [-]
Ludwik	1 330	-	0.290
Swift	1 300	0.00832	0.277

Hill yield criterion was introduced in 1948 [26]. Hill proposed an anisotropic yield criterion which includes three orthogonal symmetry planes, which is described by the following quadratic function:

$$2f(\sigma) = (G + H)\sigma_{xx}^2 + (F + H)\sigma_{yy}^2 - 2H\sigma_{xx}\sigma_{yy} + 2N\sigma_{xy}^2 \quad (3)$$

ere σ_{xx} , σ_{yy} , and σ_{zz} are stresses in the RD (x), TD (y), and thickness (z) directions, respectively; σ_{xy} , σ_{yz} , and σ_{zx} are the shear stresses in xy , yz , and zx directions. Parameters F , G , H , and N are material parameters that describe the anisotropy of the material. If $F = G = H = 1$ and $N = 3$, the Hill48 function is reduced to the von Mises criterion, or as it is called in FEM code, the Hill48 isotropic criterion. A more common description is based on normal anisotropy in the 0° , 45° , and 90° directions to the rolling direction. Then the material parameters F , G , H , and N can be described by:

$$F = \frac{r_0}{r_{90}(r_0 + 1)}, G = \frac{1}{r_0 + 1}, H = \frac{r_0}{r_0 + 1} \quad (4)$$

$$N = \frac{(r_0 + r_{90})(1 + 2r_{45})}{2r_{90}(1 + r_0)}$$

The second yield criterion used in numerical simulations was the Barlat89 yield criterion. The Barlat89 model needs three parameters for its complete formulation by which it is possible to describe the plane stress behavior. The formulation is the following [27, 28]:

$$f = a|k_1 + k_2|^M + a|k_1 - k_2|^M + (2 - a)|2k_2|^M = 2\sigma_e^M \quad (5)$$

where M is the exponent related to the crystallographic structure of the material σ_e is the initial yield stress, k_1 and k_2 can be described as:

$$k_1 = \frac{\sigma_x + h\sigma_y}{2}, k_2 = \left[\left(\frac{\sigma_x - h\sigma_y}{2} \right)^2 + p^2 \tau_{xy}^2 \right]^{1/2} \quad (6)$$

where a , h , and p are the material model parameters identified by:

$$a = \frac{2\left(\frac{\sigma_e}{\tau_{s2}}\right)^M - 2\left(1 + \frac{\sigma_e}{\sigma_{90}}\right)^M}{1 + \left(\frac{\sigma_e}{\sigma_{90}}\right)^M - \left(1 + \frac{\sigma_e}{\sigma_{90}}\right)^M}, h = \frac{\sigma_e}{\sigma_{90}}, p = \frac{\sigma_e}{\tau_{s1}} \left(\frac{2}{2a + 2^M(2 - a)} \right)^{\frac{1}{M}} \quad (7)$$

where τ_{s1} and τ_{s2} are yield stresses for two different types of shear tests: $\sigma_{12} = \tau_{s1}$ for $\sigma_{11} = \sigma_{22} = 0$ and $\sigma_{12} = 0$ for $\sigma_{22} = -\sigma_{11} = \tau_{s2}$. The identification procedure based on the coefficients r_0 and r_{90} can be also used for the identification of parameters a and h :

$$a = 2 - 2\sqrt{\frac{r_0}{1+r_0} \cdot \frac{r_{90}}{1+r_{90}}}, h = \sqrt{\frac{r_0}{1+r_0} \cdot \frac{1+r_{90}}{r_{90}}} \quad (8)$$

The coefficient p has to be calculated by a numerical procedure, by solving the non-linear equation or by using Equation (7.) instead. In our case, the coefficient p was achieved by solving the non-linear equation.

RESULTS AND DISCUSSION

This section compares and evaluates the springback results obtained from experiments and simulations. The experimental measurements focus on the arm opening angle (β) after bending, experimental values are compared with the predicted ones (Fig. 4 and Fig. 5). Given the results, it can be assumed, that yield strength of steel has a significant impact on the springback. Specimen made of TRIP RAK 40/70 steel exhibited greatest springback effect than parts made of micro alloyed H220 steel and EDDQ DC06 steel. The lowest springback effect was present on parts made of DC06 steel. Based on these results it can be stated that materials with higher values of yield strength will experience greater springback after deformation, the ratio of the total deformation to the elastic deformation is greater when material has a lower yield strength and vice versa. This assumption corresponds with the numerical results. The values of yield strength also influence bending force as shown in Tab. 7 - Tab.9. For example, bending force of RAK 40/70 steel was approximately 1.7 times higher compared to DC06 steel.

Table 7 Comparison of experimental and predicted values of bending force, arm opening angle and computation time of DC06 steel

	Bending force [N]	Arm opening angle β [°]	Computation time [s]
Experiment	260	91.2	-
Hill Ludwik	352	92.1	26.06
Barlat Ludwik	341	91.8	26.70
Hill Swift	356	92.9	26.56
Barlat Swift	321	91.9	26.68

Table 8 Comparison of experimental and predicted values of bending force, arm opening angle and computation time of H220 steel

	Bending force [N]	Arm opening angle β [°]	Computation time [s]
Experiment	330	92.9	-
Hill Ludwik	404	93.6	26.47
Barlat Ludwik	365	93.0	26.70
Hill Swift	440	94.3	26.60
Barlat Swift	321	93.2	26.69

Table 9 Comparison of experimental and predicted values of bending force, arm opening angle and computation time of RAK 40/70 steel

	Bending force [N]	Arm opening angle β [°]	Computation time [s]
Experiment	460	95.3	-
Hill Ludwik	433	95.8	27.09
Barlat Ludwik	377	95.2	27.19
Hill Swift	454	96.4	27.13
Barlat Swift	436	96.1	27.28

Yield criterion and hardening law, their impact on the springback prediction were investigated. Arm opening angle β results achieved using different yield criteria and hardening laws were compared with the experimental results in **Tab. 7 - Tab. 9**. From the given numerical results, it can be assumed, that the materials with higher yield strength (H220 and RAK 40/70) will exhibit stronger springback effect than materials with lower yield strength (DC06). When using different combinations of yield criteria (Hill and Barlat), and hardening laws (Ludwik and Swift) different values of arm opening angle β were predicted. Swift's hardening law in combination with both yield criteria predicted higher values of arm opening angle β for all materials. Better correlation with experimental results was achieved by using combination of Hill and Barlat yield criteria with Ludwik hardening law. Overall, the combination of Barlat yield criterion with Ludwik hardening law was the most accurate regarding springback prediction for all tested steels. The computation times were also compared (Tab. 7 - Tab. 9), the longest time was measured when using Barlat Swift material model and lowest time was measured for Hill Ludwik combination.

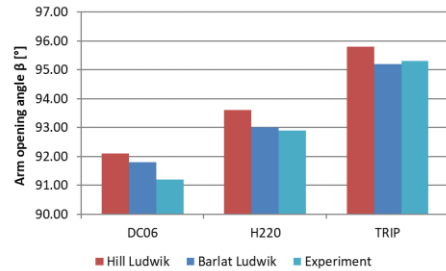


Fig. 4 Comparison of predicted Arm opening angle β [°] for all tested steels using Ludwik hardening law in combination with Hill and Barlat yield criteria

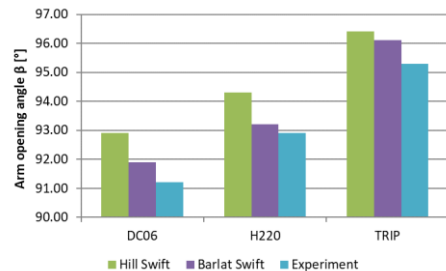


Fig. 5 Comparison of predicted Arm opening angle β [°] for all tested steels using Swift hardening law in combination with Hill and Barlat yield criteria

CONCLUSION

In this study, the impact of four material models on the springback prediction of EDDQ, HSLA and TRIP steel were evaluated in the numerical simulation. The results obtained with the use of FE analysis, forming simulations were compared with experimental ones. Based on the experimental and numerical results, the following outputs can be stated:

- Materials with higher values of yield strength (TRIP, HSLA) exhibit greater springback than materials (EDDQ) with lower yield strength.
- Hill48 and Barlat yield criteria used in combination with Ludwik hardening law indicated correlation with experimental results, the error between simulation results and experimental results was less than 1 % for all tested steels.
- Swift hardening law in combination with both yield criteria predicted higher values of the springback and bending force in all cases.
- Almost all numerical predictions overestimated springback, only in one case when simulation of bending TRIP steel using Barlat and Ludwik material model was underestimated.
- The springback predictions showed lowest error (less than 0,07 %) from experimental data when using Barlat and Ludwik material model combination in simulation.

Acknowledgements: Authors are grateful for the support of experimental works by projects APVV-21-0418, KEGA 050TUKÉ-4/2023, and VEGA 1/0539/23.

REFERENCES

1. H.L. Dai, H.J. Jiang, T. Dai, W. Xu, W.L. Luo: Journal of Alloys and Compounds, 26(708), 2017, 575–586. <https://doi.org/10.1016/j.jallcom.2017.02.270>.
2. T. Kvackaj, J. Bidulska, R. Bidulsky: Materials, 14(8), 2021, 1988. <https://doi.org/10.3390/ma14081988>.
3. E. Spisak et al.: Materials, 15(6), 2022, 2299. <https://doi.org/10.3390/ma15062299>.
4. E. Evin, M. Tomáš, S. Németh: Materials, 17(1), 2024, 210. <https://doi.org/10.3390/ma17010210>.
5. B.K. Show et al.: Materials science and Engineering, 527, 2010, 1595-1604. <https://doi.org/10.1016/j.msea.2009.10.049>.
6. L. Kascak, E. Spišák, I. Gajdoš: Acta Mechanica et Automatica, 7(2), 2013, 75-78. <https://doi.org/10.2478/ama-2013-0013>.
7. P. Mulidrán et al.: Materials, 16(2), 2023, 811. <https://doi.org/10.3390/ma16020811>.
8. L. Kascak et al.: Acta Metallurgica Slovaca, 29(4), 2023, 214–218. <https://doi.org/10.36547/ams.29.4.1979>.
9. B. Chongthairungruang, V. Uthaisangsuk: Materials and Design, 32(39), 2012, 318-328. <https://doi.org/10.1016/j.matdes.2012.02.055>.
10. J. Jeswiet, M. Geiger, U. Engel, M. Kleiner, M. Schikora, J. Dufloy: CIRP Journal of Manufacturing Science and Technology, 13, 2008, 2-17. <https://doi.org/10.1016/j.cirpj.2008.06.005>.
11. K. Lawanwong, H. Hamasaki, R. Hino, F. Yoshida: The International Journal of Advanced Manufacturing Technology, 106, 2019, 1855–1867. <https://dx.doi.org/10.1007/s00170-019-04678-y>.
12. A. Skrzat, M. Wojcik: Acta Metallurgica Slovaca, 29(4), 2023, 200–205. <https://doi.org/10.36547/ams.29.4.1949>.
13. J. Slota, E. Spišák: Metalurgija, 47(1), 2008, 13-17.
14. J. Slota, M. Šiser, M. Dvorák: Strength of Materials, 4, 2017, 93-102. <https://doi.org/10.1007/s11223-017-9900-6>.
15. T. Yoshida, K. Sato, E. Isogai, K. Hashimoto: Springback problems in forming of High-Strength steel sheets and countermeasures. Nippon steel technical report, 103, 2013, 4-10.
16. M. Samuel: Journal of material processing technology, 105, 2013, 382-393. [https://doi.org/10.1016/S0924-0136\(00\)00587-2](https://doi.org/10.1016/S0924-0136(00)00587-2).
17. P. Mulidrán, M. Šiser, J. Slota, E. Spišák, T. Slezziak: Metals, 8(6), 2018, 435. <https://doi.org/10.3390/met8060435>.
18. D. Neto, M. Oliveira, A.D. Santos, J. Alves, L.F. Menezes: International Journal of Mechanical Sciences, 122, 2017, 244–254. <https://doi.org/10.1016/j.ijmecsci.2017.01.037>.
19. J. Slota, M. Jurčičin, L. Lázárescu: Acta Metallurgica Slovaca, 20, 2014, 236–243. <https://doi.org/10.12776/ams.v20i2.287>.
20. K. Seo, J. Kim, H. Lee, J.H. Kim, B. Kim: Metals, 18 (8), 2017. <https://doi.org/10.4271/2002-01-0159>.
21. W.A.B. Baara, B. Baharudin, M. Ariffin, M. Ismail: Metals, 9, 2019, 511. <https://doi.org/10.3390/met9050511>.
22. X. Cui, A. Xiao, Z. Du, Z. Yan, H. Yu: Metals, 10, 2020, 390. <https://doi.org/10.3390/met10030390>.
23. P. Mulidrán, E. Spišák, M. Tomáš, V. Rohaľ, F. Stachowicz: Acta Mechanica Slovaca, 23 (4), 2019, 14-18. <https://doi.org/10.21496/ams.2019.022>.
24. E. Evin, M. Tomáš: Acta Metallurgica Slovaca, 25 (4), 2019, 208-216. <https://doi.org/10.12776/ams.v25i4.1362>.
25. T. Trzpiecinski et al.: Acta Metallurgica Slovaca, 29(3), 2023, 123–129. <https://doi.org/10.36547/ams.29.3.1780>.
26. R. Hill: Proceedings of the royal society A. 1948, 193, 281–297.
27. S. Bruschi, T. Altan, D. Banabic, P. Bariani, A. Brosius, J. Cao, A. Ghiotti, M. Khraisheh, M. Merklein: CIRP Annals, 63, 2014, 727–749. <https://doi.org/10.1016/j.cirp.2014.05.005>.
28. F. Barlat, J. Brem, J.W. Yoon, K. Chung, R. Dick, D. Lege: International Journal of Plasticity, 19, 2003, 1297–1319. [https://doi.org/10.1016/S0749-6419\(02\)00019-0](https://doi.org/10.1016/S0749-6419(02)00019-0).